Article

MaP Peptides: Programming the Self-Assembly of Peptide-Based Mesoscopic Matrices

Maxim G. Ryadnov, and Derek N. Woolfson

J. Am. Chem. Soc., **2005**, 127 (35), 12407-12415• DOI: 10.1021/ja052972i • Publication Date (Web): 12 August 2005

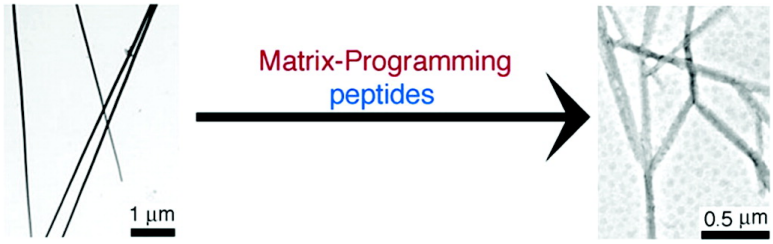

More About This Article

Additional resources and features associated with this article are available within the HTML version:

- Supporting Information
- Links to the 10 articles that cite this article, as of the time of this article download
- Access to high resolution figures
- Links to articles and content related to this article
- Copyright permission to reproduce figures and/or text from this article

View the Full Text HTML

J|A|C|S
ARTICLES
Published on Web 08/12/2005

MaP Peptides: Programming the Self-Assembly of Peptide-Based Mesoscopic Matrices

Maxim G. Ryadnov† and Derek N. Woolfson*,†

Contribution from the Department of Biochemistry, School of Life Sciences, University of Sussex, Falmer, BN1 9QG, United Kingdom

Received May 6, 2005; E-mail: chdnw@bristol.ac.uk

Abstract: We describe an approach that utilizes nonlinear peptides to direct the assembly of previously reported Self-Assembling Fibers (SAFs). The SAF system comprises two complementary linear peptides, SAF-p1 and SAF-p2a, which combine to form exclusively linear, nonbranched fibers. The Matrix-Programming (MaP) peptides described herein are based on these peptides: they comprise two or three half-peptide blocks derived from the SAF peptides, which are conjugated via dendritic hubs. Different MaP peptides coassembled with the standard SAF peptides to form specific structures, such as hyperbranched networks, polygonal matrices, and regularly segmented and terminated fibers. The role of each half-peptide block in dictating the different features has been elucidated. This provides a strong basis for designing new peptide-based nanostructured materials from the bottom up.

Introduction

An array of nanometer-to-micron scale structures covering a broad range of chemical types, structural morphologies, and functions are being developed.[1] The drive for this is (1) understanding molecular self-assembly and organization and (2) developing a potentially diverse set of technological applications that require supramolecular structures and materials defined and controlled at the molecular level.[2] The realization of these depends on finding precise ways to synthesize or assemble such structures. Molecular self-assembly is widely recognized as a potential route to advancing this approach.[3,4] Using small molecules as building blocks, self-assembly allows well-defined polymolecular suprastructures to be fabricated and stabilized by large networks of noncovalent interactions. In other words, assembly is from the bottom up, being programmed into the molecular building blocks. Biological assemblies provide numerous examples of this type of assembly and inspiration for the design and engineering of synthetic self-assembling systems.

Among the most eagerly awaited mesoscopic structures are matrices, i.e., complex polymolecular systems that can support, template, or deliver other entities.[5−8] For instance, there is increasing interest in fabricating materials such as nanowire networks,[5,6] affinity matrices,[7] and artificial mimics of extracellular matrices to support cell growth.[8] One advantage of defined self-assembled matrices, as compared to aggregates of polymeric molecules, is their ability to sustain the morphology and topology initially programmed through their interconnections. In this context, natural and synthetic matrices described to date can be divided into two major classes: polymolecular and supramolecular. Polymolecular matrices are predominately covalent and employ various types of polymer to form intricate networks,[9,10] including peptide-driven self-assembly of polymer-peptide hybrids.[11,12] The supramolecular types use noncovalent interactions to drive matrix formation. As introduced above, molecular self-assembly provides a potential solution for this. Self-assembling collagen and fibrin networks represent naturally occurring examples of matrices, and peptide-based self-assembling fibers[13] are among the synthetic examples.

Like some others,[13,14] our efforts have focused on synthetic peptides that self-assemble to form fibrous systems[15] as mimics

† Current address: School of Chemistry, University of Bristol, Bristol, BS8 1TS, UK.

(1) (a) Whitesides, G. M. *Nat. Biotechnol.* **2003**, *10*, 1161−1165. (b) MacPhee, C. E.; Woolfson, D. N. *Curr. Opin. Solid State Mater. Sci.* **2004**, *8*, 141−149.
(2) Lowe, C. R. *Curr. Opin. Struct. Biol.* **2000**, *10*, 428−434.
(3) Whitesides, G. M.; Mathias, J. P.; Seto, C. T. *Science* **1991**, *254*, 1312−1309.
(4) Elemans, J. A.; Rowan, A. E.; Nolte, R. J. *J. Mater. Chem.* **2003**, *13*, 2661−2670.
(5) Huang, Y.; Duan, X.; Wei, Q.; Lieber, C. M. *Science* **2001**, *291*, 630−633.
(6) Adelung, R.; Aktas, O. C.; Franc, J.; Biswas, A.; Kunz, R.; Elbahri, M.; Kanzow, J.; Schurmann, U.; Faupel, F. *Nat. Mater.* **2004**, *6*, 375−379.
(7) Moll, D.; Huber, C.; Schlegel, B.; Pum, D.; Sleytr, U. B.; Sara, M. *Proc. Natl. Acad. Sci. U.S.A.* **2002**, *99*, 14646−14651.
(8) Hubbell, J. A. *Curr. Opin. Biotechnol.* **2003**, *14*, 551−558.
(9) Nowak, A. P.; Breedveld, V.; Pakstis, L.; Ozbas, B.; Pine, D. J.; Pochan, D.; Deming, T. J. *Nature* **2002**, *417*, 424−428.
(10) Wang, Y.; Ameer, G. A.; Sheppard, B. J.; Langer, R. *Nat. Biotechnol.* **2002**, *20*, 602−606.
(11) Petka, W. A.; Harden, J. L.; McGrath, K. P.; Wirtz, D.; Tirrell, D. A. *Science* **1998**, *281*, 389−392.
(12) Wang, C.; Stewart, R. J.; Kopecek, J. *Nature* **1999**, *397*, 417−420.
(13) Hartgerink, J. D.; Beniash, E.; Stupp, S. I. *Science* **2001**, *294*, 1684−1688.
(14) (a) Potekhin, S. A.; Melnik, T. N.; Popov, V.; Lanina, N. F.; Vazina, A. A.; Rigler, P.; Verdini, A. S.; Corradin, G.; Kajava, A. V. *Chem. Biol.* **2001**, *8*, 1025−1032. (b) Marini, D. M.; Hwang, W.; Lauffenburger, D. A.; Zhang, S.; Kamm, R. D. *Nano Lett.* **2002**, *2*, 295−299. (c) Aggeli, A.; Nyrkova, I. A.; Bell, M.; Harding, R.; Carrick, L.; McLeish, T. C.; Semenov, A. N.; Boden, N. *Proc. Natl. Acad. Sci. U.S.A.* **2001**, *98*, 11857−11862. (d) Zhou, M.; Bentley, D.; Ghosh, I. *J. Am. Chem. Soc.* **2004**, *126*, 734−735. (e) Zimenkov, Y.; Conticello, V. P.; Guo, L.; Thiyagarajan, P. *Tetrahedron* **2004**, *60*, 7237−7246.
(15) (a) Ryadnov, M. G.; Woolfson, D. N. *Nat. Mater.* **2003**, *2*, 329−332. (b) Ryadnov, M. G.; Woolfson, D. N. *Angew. Chem., Int. Ed.* **2003**, *42*, 3021−3023. (c) Ryadnov, M. G.; Woolfson, D. N. *J. Am. Chem. Soc.* **2004**, *126*, 7454−7455.

of protein-based fibers. However, as with many synthetic cases, fibrillogenesis does not lead to the formation of meshes and networks directly and requires additional means to provide fiber interconnections. In some other systems this has been achieved by the covalent cross-linking of individual fibers.[13] Alternatively, network assembly could be programmed during fibrillogenesis. To our knowledge and surprisingly, examples of the latter have not been described. However, an ability to induce and control the formation of supramolecular networks purely by noncovalent means would be of considerable interest and would impact on nanoscience and technology. With this in mind, we set out to produce a novel synthetic supramolecular matrix formed by noncovalently linked peptide-based fibers. This was based on our own self-assembling fiber (SAF) system.[16]

An Introduction to the SAF System. The SAF system comprises two linear peptides of de novo design, SAF-p1 and SAF-p2. The design rationale is as follows: the peptides complement each other to form a parallel heterodimeric coiled coil with overhanging "sticky ends". These ends nucleate longitudinal assembly of the dimer to form protofibrils, which would be expected to have a width of ~2 nm. In practice, however, the protofibrils associate laterally (i.e., they bundle) to form mesoscopic fibers, ≥40 nm thick and tens of microns long. The details of the design are as follows:[16] both SAF peptides are 28-residue, linear peptides comprising proteinogenic amino acids only; they are based on the archetypal coiled-coil dimer, namely the leucine-zipper motif, and comprise four contiguous heptad repeats, ***abcdefg***, along their sequences; to foster the formation of a coiled-coil dimer, the hydrophobic core ***a*** and ***d*** positions are mostly Ile and all Leu, respectively; each peptide has a basic N-terminal half (with ***e*** = ***g*** = Lys) and an acidic C-terminal half (***e*** = ***g*** = Glu) to promote staggered assembly; finally, to cement the stagger further, each peptide has a single Asn at a different ***a*** site. The significance of these Asn inclusions is that their amide side chains must be satisfied by hydrogen-bonding interactions when located within a coiled-coil core; placing another complementary Asn in the partnering coiled-coil strand achieves this and also imparts dimer specificity.[15−19] We refer to the originally described peptides as SAF-p1 and SAF-p2[16] but now largely work with a modified version of SAF-p2, named SAF-p2a, which combines with SAF-p1 to assembled yield fibers of improved stability.[15,17]

Recent Redesigns Based on the SAF System. Through subtle changes to the peptide design it has been possible to rationally improve the physical properties of the SAFs, namely, with respect to the thermal, salt, and pH stability.[15,17] Though it also is possible to relax the supramolecular rigidity of the assemblies to some extent, the redesigned fibers remain straight, nonbranched, rod-like structures.[15−17] Thus, the exclusive use of linear SAF peptides does not provide the necessary versatility to alter fiber shape rationally. We reasoned that this would best be done by intervening early in the assembly process and, particularly, prior to the formation of the matured, thickened fibers: according to our working model for assembly, Figure 1A,[16−18] the critical point in fibrillogenesis is the rapid formation of coiled-coil protofilaments, which present the least energetic and steric restraints for accommodating nonstandard SAF-based peptides. Thus, our premise has been to design *special peptides* that complement the *standard*, linear SAF peptides. These could be added to SAF mixtures during the initial preparation so that they are incorporated directly during SAF fibrillogenesis. The aim being to influence protofibril structure and, consequently, the organization of matured fibers.

To this end, we first designed T-shaped peptides in which half-peptide units are attached to standard SAF peptides via the side chain of a central, exposed Lys. The aim was to promote orthogonal protofilament assembly and facilitate branching, Figure 1B. Although branching is observed, the T-shaped constructs are not entirely compatible with the SAF system and only gave low branching densities.[15b] To overcome this problem we constructed other special peptides (1) to better complement the standard SAFs; (2) to incorporate and redirect the assembly of protofilaments; and (3) to influence fiber morphology and function. This led to a new concept in protein fibrillogenesis, which we call Fiber Shaping (FiSh).[15a] Specifically, we have recently reported two FiSh peptides, C_2^N and D_2^C, that introduce kinks/waves and splits/branches into the fibers, respectively.[15a] Each peptide is designed to ensure the incorporation of just one FiSh molecule per protofilament to act as a nucleator or director of alternative assembly. This is achieved by duplicating two identical half-peptide fragments derived from the standard SAF sequences in a head-to-head or a tail-to-tail fashion. The fragments are dubbed A^N and B^C for SAF-p1 and C^N and D^C for SAF-p2a (Figure 1). In the original design for the sticky ended dimer, A^N is the N-terminal half of SAF-p1 and complements D^C, the C-terminal half of SAF-p2a. Similarly, C^N is the N-terminal half of SAF-p2a and complements B^C, the C-terminal half of SAF-p1. In designing FiSh constructs two main principles are followed: first, any half-sized SAF fragment used has to retain the same terminus that is free in the corresponding parent SAF peptide. In the case of the aforementioned C_2^N and D_2^C, the N-terminus of C (hence the N superscript) and the C-terminus of D (C superscript) were free, while the other termini were used to link the blocks to the spacer (Figure 1C). Peptides made against this rule terminate fibrillogenesis leading to unrectifiable disruptions in the fibers.[15a] Second, for the original FiSh constructs the building blocks are the same, e.g., both C^N or both D^C, with the number of blocks being indicated by subscripts. Such peptides are accommodated by the standard linear SAFs and set up convergent and divergent modes of fiber assembly resulting in kinking and splitting the fibers.[15a]

Based on these descriptions of SAF assembly, we aimed to design further specialist peptides capable of driving the fibers into interconnecting networks, i.e., supramolecular matrices. We describe these peptides here and refer to them as Matrix-Programming (MaP) peptides, Figure 1D.

Results and Discussion

Design Principles. One particular feature of natural matrices formed by fibrillar proteins is branching. Though one of our previously described FiSh peptides does cause the SAFs to split at a high rate, it does not produce cross-links (i.e., branches

(16) Pandya, M. J.; Spooner, G. M.; Sunde, M.; Thorpe, J. R.; Rodger, A.; Woolfson, D. N. *Biochemistry* **2000**, *39*, 8728−8734.
(17) Smith, A. M. Ph.D. Thesis, University of Sussex, 2003.
(18) Smith, A. M.; Acquah, S. F.; Bone, N.; Kroto, H. W.; Ryadnov, M. G.; Stevens, M. S.; Walton, D. R.; Woolfson, D. N. *Angew. Chem., Int. Ed.* **2005**, *44*, 325−328.
(19) (a) Gonzalez, L., Jr.; Woolfson, D. N.; Alber, T. *Nat. Struct. Biol.* **1996**, *3*, 1011−1018. (b) Woolfson, D. N. *Curr. Opin. Struct. Biol.* **2001**, *11*, 464−471.

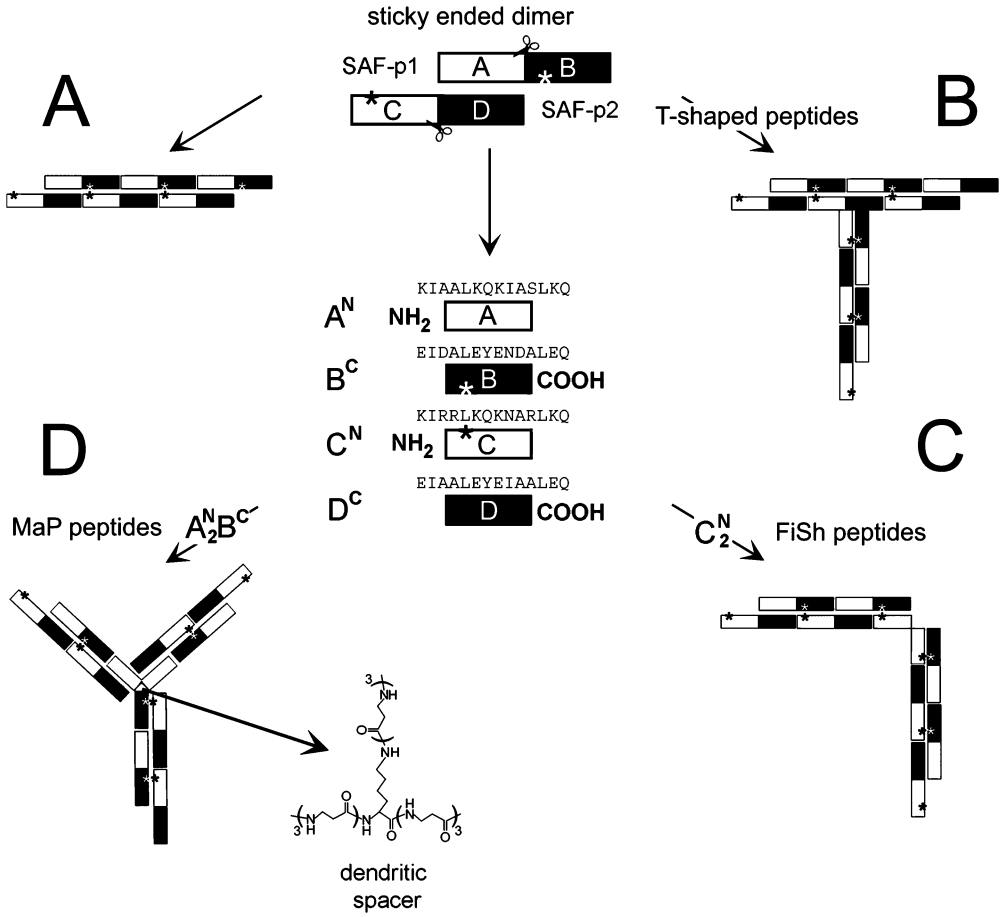

Figure 1. Scheme illustrating the Self-Assembling Fiber (SAF) system, T-shaped, Fiber-Shaping (FiSh), and Matrix-Programming (MaP) peptide designs. (A) *Standard assembly*. Two SAF peptides complement to form sticky ended dimers, which assemble into coiled-coil protofibrils. *N.B., in practice, these protofibrils bundle* further to form matured thickened fibers. (B) *Branched assembly*. T-shaped peptides can be mixed with standard SAF peptides to set up orthogonal assembly of protofibrils resulting in branched fibers.[15b] (C and D) Each SAF peptide has two chemically distinct halves designated A^N and B^C and C^N and D^C. The superscripts indicate the terminus that is free in the full-length parent SAF peptide. (C) *Kinked assembly*. The FiSh peptide, C_2^N, seeds convergent assembly of protofibrils which results in kinked fibers.[15a] (D) *Hyperbranched and networked assembly*. The tridirectional peptides, such as $A_2^NB^C$, described herein were built around dendritic spacers (1) to allow better accommodation into SAFs and (2) to produce more complex morphologies.

shared by two or more separate fibers) and is, therefore, of limited use in making matrices.[15a] Moreover, the branches formed are short. Branch length can be improved by using T-shaped peptides; however, the incorporation of these peptides into SAFs is not tolerated very well resulting in a low density of branches.[15b] We took these observations into consideration in designing the first MaP peptides.

The first MaP designs combined positive aspects of both previous designs: i.e., (1) that the FiSh peptides are tolerated in SAF assembly and give high branching densities and (2) that the T-shaped constructs give extended branches of comparable length to normal fibers. In some respects, the first MaP peptides followed a similar structural template used for the FiSh peptides; namely, half-sized SAF peptides were linked through flexible joints.[15a] However, to introduce and improve branching the capacity for a third limb was added to make orthogonal trimeric MaP peptides (Figure 1D). In addition, a dendrimeric spacer was designed to give additional flexibility to the MaP peptides (Figure 1D).

Promoting Hyperbranching. To test the above principles, we synthesized $C_2^ND^C$. Following the main design principles for the FiSh peptides,[15a] $C_2^ND^C$ used C_2^N to open an angle in the otherwise straight SAFs (i.e., it aimed to kink the protofibrils and fibers) and D^C to introduce potential branching sites. The effect of the $C_2^ND^C$ design was assessed by comparing Transmission Electron Microscopy (TEM) images of fibers assembled from standard SAF mixtures containing $C_2^ND^C$ or D_2^C, Figure 2A and B, respectively. In both cases, branches were apparent. The selected images show unfinished or embryonic branches, which, if fibrillogenesis had been left for longer, would have matured. The point of these images is to demonstrate the different spur angles resulting from the incorporation of different *special* peptides: for the D_2^C-containing (an original FiSh construct) fibers, the growth of branches was spatially restricted, Figure 2B; in contrast, the use of a kink-producer, C_2^N, in $C_2^ND^C$ (an MaP construct) eliminated this restriction, presumably by opening up an angle at the kink as desired (Figure 2A).

In the proof-of-principle design of $C_2^ND^C$, we expected some competition between kinking and branching, which was observed: branched fibers were found of normal size ($\geq$50 nm wide and tens of microns long) resembling those formed by previously reported T-shaped peptides[15b] and with branching frequencies close to that previously reported for D_2^C-containing fibers (Figure 2C).[15a] However, kinked fibers were also present and even dominated some preparations; indeed, it was not possible to assess with any certainty the branch-to-kink ratio, which varied with preparation.

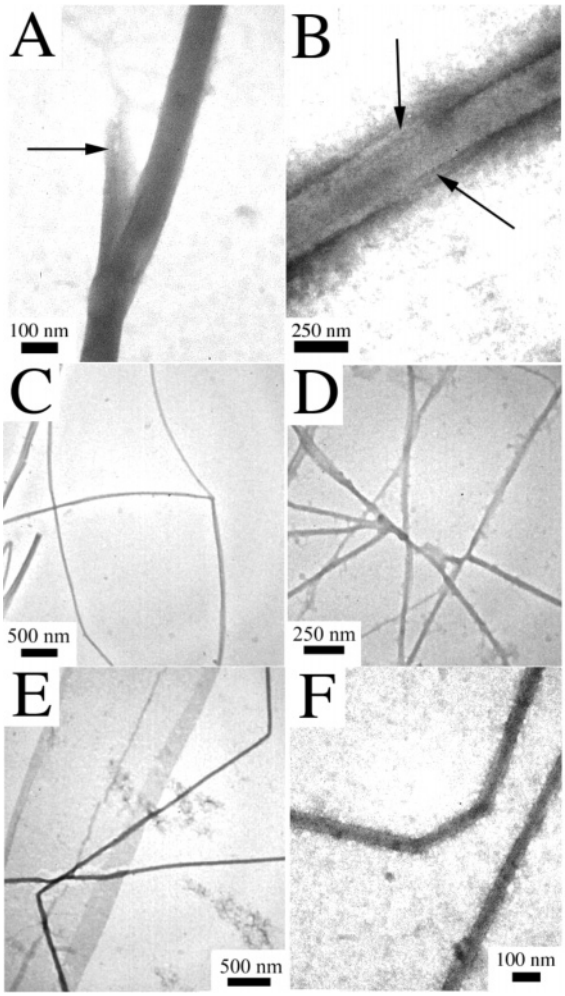

Figure 2. Electron micrographs of SAFs with MaP inclusions. Unfinished branches spurred at different angles from the fibers, which resulted from the coassembly of the standard SAF peptides with the MaP peptide, $C_2^ND^C$ (A), and the FiSh peptide, D_2^C (B). Full branches formed in the presence of the MaP peptides, $C_2^ND^C$ (C) and $A_2^NB^C$ (D). Kinks introduced by the MaP homotrimers, C_3^N (E) and A_3^N (F).

This competition between kinking and branching may be attributed to an aforementioned feature of sticky-ended design, namely the inclusion of asparagine residues at the coiled-coil interface. Such asparagines give coiled coils high selectivity, discriminating against alternative assemblies.[19] In $C_2^ND^C$, two of the three blocks (the C^N blocks) have these asparagine residues. In light of this, the behavior of the peptide is consistent with that of the FiSh peptides. To test further if asparagine residues affected the branch-to-kink ratio, we made another MaP peptide, $A_2^NB^C$, using the subunits of the other standard SAF peptide. This peptide has just one block (B^C) with an interfacial asparagine. Consistent with this, $A_2^NB^C$ considerably shifted the branch-to-kink ratio to the branch side (Figure 2D). Further support for this model came from two other MaP peptides, C_3^N and A_3^N. With interfacial asparagine residues in all three blocks, the homotrimeric C_3^N was expected to be extremely selective in its interactions (see below for an argument for this). Indeed, C_3^N showed marginal kinking as compared to C_2^N (Figure 2E), while A_3^N showed both branching (not shown) and kinking (Figure 2F), but without preference for either. The similar behavior of the homotrimers must result from their chemical nature. Both constructs are conjugates of one positively charged block, which gives large positive net charges to both, C_3^N (+24) and A_3^N (+15), compared with those for the heterotrimers, $C_2^ND^C$ (+9) and $A_2^NB^C$ (+3). Recently, we showed that charge does play a defining role in the SAF system.[18] As the standard sticky-ended dimer has an overall charge of +1, any incorporated MaP homotrimers may affect further assembly considerably. We hypothesize that the homotrimers are less suited in the SAF system than their dimeric counterparts. In other words, the homotrimers are not effective in incorporating all three blocks into the hierarchy of the SAF assembly, with one block being structurally redundant. Consistent with this, the less-charged dimeric A_2^N peptide was found to produce both kinking and splitting like D_2^C (data not shown). This supports the empirical observation that, among all peptides described so far, only $A_2^NB^C$ supports hyperbranching of extended fibers resembling network formation (Figure 2D). This behavior appears to be mainly attributable to the A_2^N component causing splits and kinks concomitantly. At these sites, the B^C block may be acting similarly to D^C in $C_2^ND^C$ in forming extended branches. Nonetheless, the precise role of the B^C block remained unclear, which prompted the following experiments.

Intermitted Assembly and Segmented Fibers. The B^C block complements C^N. Both blocks contain interfacial asparagine residues, which, along with their opposite overall charges, makes the B^C:C^N interaction highly specific. As a result, two copies of C^N linked in C_2^N produce exclusively one morphological feature, namely kinked fibers. On the other hand, D_2^C lacks the interfacial asparagines and produces two features (kinks and splits).[15a] We propose that this may lead to more promiscuity in binding of this block, and, likewise, with block A^N, in inter-SAF peptide interactions. B^C is negatively charged and essentially the same as D^C, but with an interfacial asparagine. Thus, interactions made by B^C are expected to be weaker than those made by D^C, but more specific like those made by C^N. This could possibly result in another unique morphological feature introduced by B^C.

To test the behavior of the B^C subunit, we made a comparative version of $A_2^NB^C$, namely $A^NB_2^C$. According to our developing model, this peptide should have produced significantly less branching and kinking compared with $A_2^NB^C$, as the efficiency of these processes had been ascribed to A^N.[15a] Branching and kinking were indeed impaired with SAF preparations that included $A^NB_2^C$. Moreover, a novel and intriguing feature of the $A^NB_2^C$-containing fibers emerged: the fibers were mostly segmented (Figure 3A). We suspected that the B^C block somehow restricted fiber assembly. To test this, we made B_2^C. Doping B_2^C into SAF mixtures resulted in regularly segmented fibers without branches or kinks (Figure 3B and C).

Analysis of the TEM images of B_2^C-containing SAF samples revealed that the segments were uniformly sized and separated: the distances between the segments and their lengths varied for different samples but did not exceed 100 nm and 2 μm, respectively (Figure 3B and C). We suspect that the blockage of C^N units in most protofibrils by B_2^C weakens the fibers, which results in partial breakage (segmentation) during preparation for TEM (Figure 3C and Experimental Section). In this respect, the almost uniform size of the segments is interesting. Though this needs further detailed study, our working hypothesis is that the B_2^C units incorporate at some

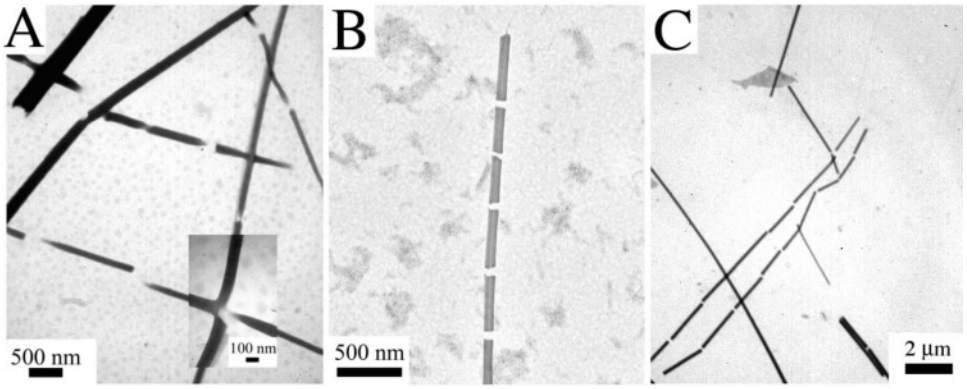

Figure 3. Electron micrographs of segmented SAF fibers assembled in the presence of $A^NB_2^C$ (A) and B_2^C (B, C) in stoichiometric ratios with the standard SAF peptides.

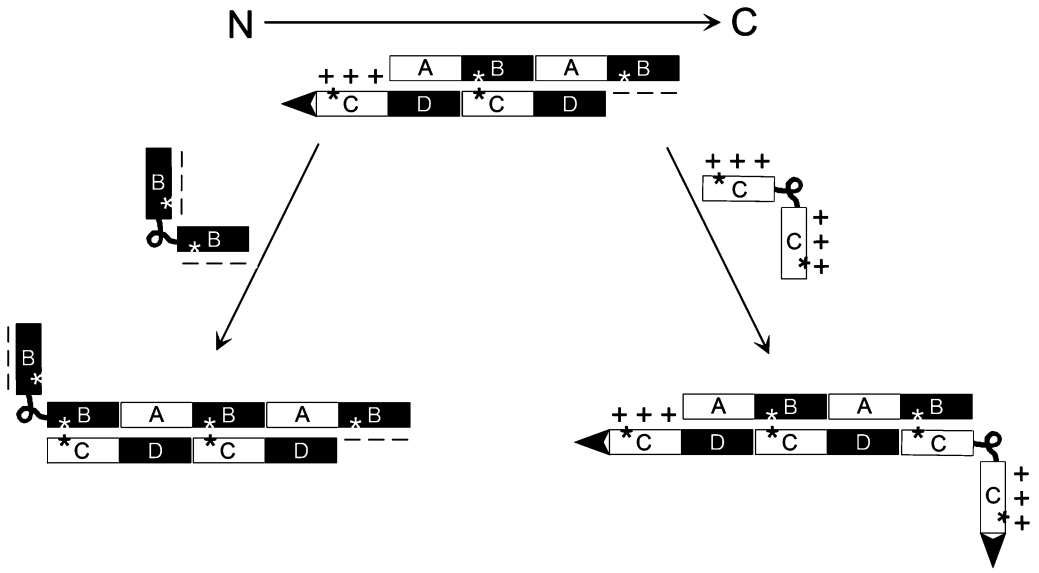

Figure 4. Unidirectional assembly of SAF fibers with the growing positively charged ends (top). B_2^C acidifies the end (left), and C_2^N introduces a second potential growing end (right).

regular rate into fibers that is much slower than that for the incorporation of the standard peptides, SAF-p1 and SAF-p2a.

Expanding a Working Model for SAF Fibrillogenesis. The segmented fibers are consistent with our latest observations on the polar nature of SAF fibrillogenesis.[18] In the original SAF design the order of addition of SAF-p1 and SAF-p2a is set, which results in polar protofibrils. As a result, B_2^C can only add to the ends of protofibrils that have overhanging C^N blocks from the standard linear peptides; whereas, C_2^N will add to ends with overhanging B^C blocks. One possible model for SAF assembly is depicted in Figure 4, where there are two oppositely charged potential growing ends of the protofibrils. The question is what sets the difference of morphological features in fibers introduced by B_2^C and C_2^N? We posit that the preferred growing end of the protofibrils is that presenting C^N blocks, which is the end to which B_2^C must add. This sets up unidirectional assembly, which is consistent with our observations that matured fibers are tapered at one end and thick and blunt at the other (unpublished data) and that labeled SAF-p2a preferentially adds to one end of such fibers.[18] Furthermore, according to the model in Figure 4, the addition of B_2^C converts the C^N end to B^C partially stopping the growth of protofibrils; while C_2^N does the opposite creating a new growing end which is not necessarily contiguous with the fiber axis (Figure 4). Consistent with this, C_2^N introduces the divergent mode of assembly and produces kinked fibers. Finally, because both B^C and C^N blocks are very selective in binding, B_2^C and C_2^N each introduce one dominating morphological feature into fibers, namely, intermissions and kinks, respectively.

N.B. the alternative model with overhanging A^N and D^C blocks is less likely as these blocks do not have asparagines and should form more stable coiled-coil interactions comparably quicker to nucleate fibrillogenesis and leave B^C and C^N overhangs; i.e., the A^N and D^C blocks effectively become sequestered within the coiled-coil protofibrils and fibers and are rarely (if at all) available at the ends of the structures to propagate fibrillogenesis. On the basis of this kinetic argument, any free A_2^N- and D_2^C-containing peptides may also be less selective in binding. They may even interact with oppositely charged B^C and C^N blocks, respectively, at the ends of fibrous structures to produce more than one feature (e.g., kinks and splits), though we recognize that such interactions would be compromised to some extent by the burial of a single asparagine per interaction. In the case of $A^NB_2^C$, the B^C blocks cause fibrillogenesis to intermit, while the A^N block facilitates branching (Figure 3A).

Arranging Polygonal Fibrous Networks. Thus far, we have considered only MaP peptides composed of units from the same

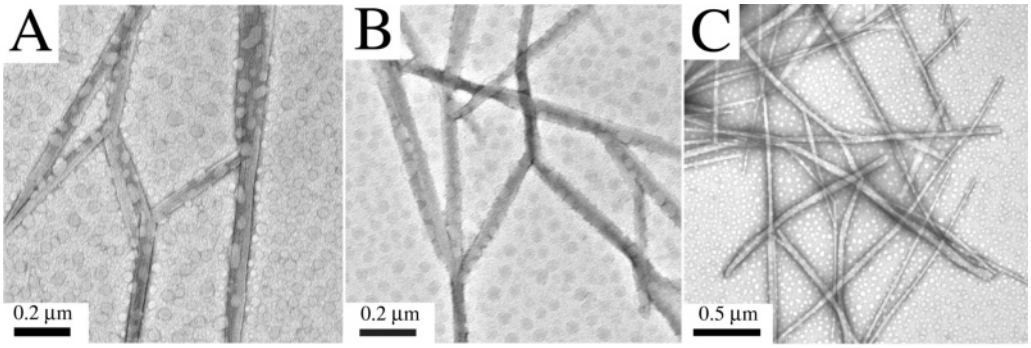

Figure 5. Electron micrographs of interconnected SAF networks assembled using a 1:1:1 ratio of SAF-p1, SAF-p2a, and the MaP peptide A^NC^N.

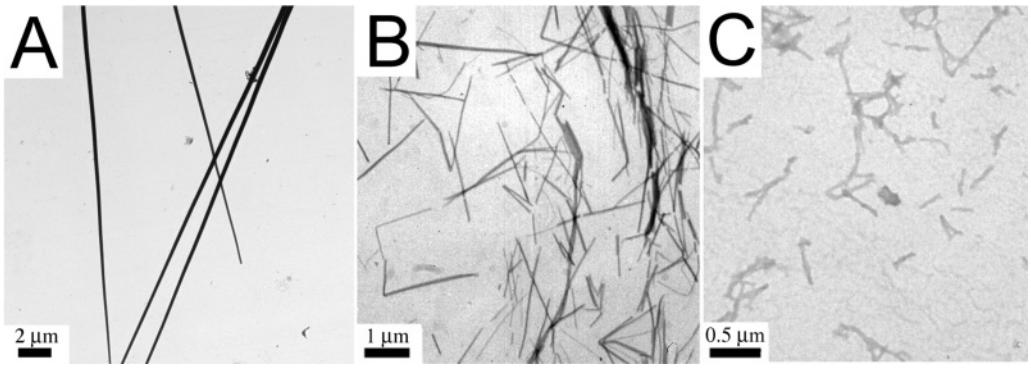

Figure 6. Electron micrographs of SAF fibers assembled at standard conditions (A) and inhibited by $C_2^NC^C$ (B) and $C^NC^CD^N$ (C) at 0.1:1 ratios to SAF peptides.

SAF peptide, either SAF-p1 or SAF-p2a. These gave encouraging results toward the goal of making networks, the best being achieved using $A_2^NB^C$, which gives hyperbranched fibers (Figure 2D). However, the resulting fibers lacked regularity, and not all were branched or involved in cross-linking. To overcome this and to foster the binding of MaP peptides to both SAFs, we made the hybrid peptide, A^NC^N. Though A^NC^N is structurally more similar to FiSh dimers than MaP trimers, its desired role was to provide or increase interprotofibril links and, hence, interfiber connections: unlike the other FiSh and MaP peptides, A^NC^N combines blocks from both SAFs and, therefore, has the potential to link complementary subunits from different protofibrils during fibrillogenesis. Consistent with this, A^NC^N predominantly produced fibers that were interconnected in microscopic networks (Figure 5).

Terminating Fibrillogenesis. All of the peptides described so far propagated fibrillogenesis of the SAFs, albeit in some unusual way. It is also of interest to control and limit fibrillogenesis through termination. As we have shown previously,[15a,b] dimeric FiSh and T-shaped terminators can be designed to stop fibrillogenesis. To continue this theme and to make more-efficient terminators, we designed the following MaP-based constructs: as an alternative to $C_2^ND^C$, we made $C_2^NC^C$. This peptide was designed to produce shortened and/or defective fibers without necessarily terminating fibrillogenesis completely, as it incorporates the C_2^N block to propagate and the C^C to terminate. At up to stoichiometric ratios with standard SAFs, $C_2^NC^C$ did give shortened fibers (Figure 6B). Some kinking, but no branching, was also apparent supporting our proposal on the role of C_2^N. To attempt complete inhibition, we made $C^NC^CD^N$ in which both C^C and D^N should act as terminating blocks. Indeed, ratios as low as 0.1:1:1 of $C^NC^CD^N$ to SAF-p1 and SAF-p2a inhibited fiber growth (Figure 6C), and stoichiometric ratios completely terminated fibrillogenesis. These results provide additional support for the MaP concept and the use of specialist peptides in engineering and controlling the SAF system. Specifically, these results suggest routes to achieving better control over the fiber assembly without changing the physical conditions for fibrillogenesis (e.g., temperature, pH, and salinity).

Structural and Stability Costs Associated with the Incorporating MaP Peptides. So far we have shown that all four blocks from the SAF peptides can be specifically designed into specialist constructs to produce different modes of fibrillogenesis. This confers a powerful and predictable system to rationally program the architecture of fibrous scaffolds. Remarkably, at the microscopic level at least, all of the SAF−MaP mixtures displayed similar underlying fibrous structures. One question that remains, however, is whether the underlying α-helical organization of the SAFs is conserved upon MaP incorporation. This was addressed using circular dichroism (CD) and Fourier transform infrared (FT-IR) spectroscopies.

CD spectra of the assembled standard SAFs are somewhat unusual but, nonetheless, are consistent with α-helical structure:[16] the spectra have minima at 208 and 222 nm; and, although the 222 nm band is slightly red shifted and the 208 nm band is reduced in intensity, these features are characteristic for particulate systems exhibiting light scattering.[16] CD spectra of A^NC^N-containing SAF samples showed a further red shift and complete disappearance of the minimum at 208 nm (Figure 7A) suggesting large assemblies, consistent with the TEM images (Figure 5). However, the intensity of the CD signal at 222 nm for MaP-containing samples was comparable with those for the standard SAF fibers alone (Figure 7A).

As a result of the loss of the 208 nm signal, the overall shape of the CD spectra resembled that expected for a β-sheet. To be

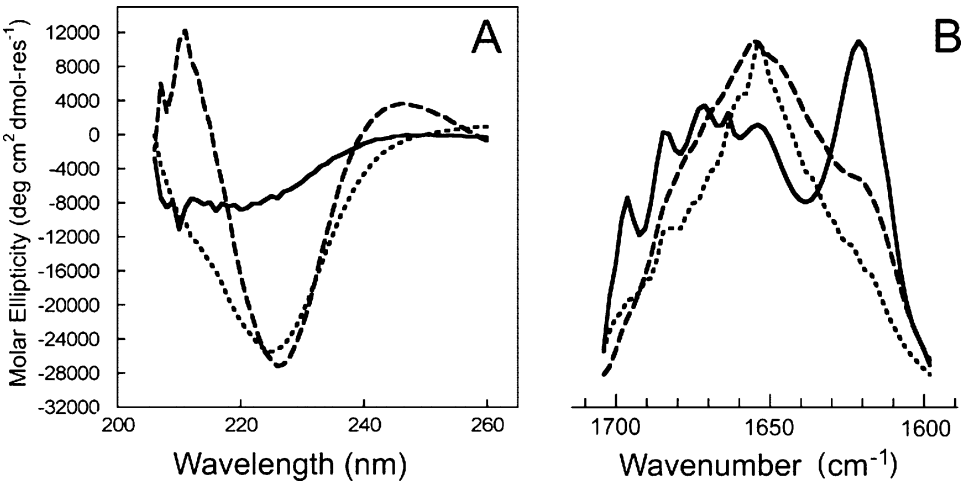

Figure 7. CD (A) and FT-IR (B) spectra of standard SAF and SAF−A^{N}C^N fibers. SAF (dotted line) and SAF-A^{N}C^N (dashed line) fibers assembled under standard conditions; SAF−A^{N}C^N (solid line) cooled after thermal denaturation.

sure that we had not compromised the underlying α-helical architecture of the SAFs, we compared SAF and SAF-MaP preparations by FT-IR spectroscopy. The spectra for all the preparations were dominated by peaks around 1650 cm^{-1}, which are characteristic of α-helices (Figure 7B). However, a less intense band at 1610−1625 cm^{-1} normally associated with intermolecular β-aggregates[20] was also apparent for the SAF−MaP mixtures (Figure 7B). Although some coiled-coil proteins have been reported to give an unusual band at ∼1630 cm^{-1} in addition to the major band at 1650 cm^{-1},[20b] we sought additional data on the SAF−MaP preparations, namely the binding of Congo Red.[21] Fibers rich in β-sheet, such as amyloid, bind Congo Red to give a yellow-green color in cross-polarized light. Although the standard SAF fibers did bind Congo Red, the resulting color was not yellow-green but red-gold (Figure 8A). We propose that this binding to the SAFs is due to the highly basic and regular nature of the fibers, which provides extensive possibility for multiple electrostatic interactions with the sulfonated Congo Red.[22] Also, the dye has been reported to bind native proteins regardless of their secondary structure suggesting that there is no absolute structural prerequisite for binding.[22b] In this context, we suggest that Congo Red binds the SAFs and is anisotropically aligned by the highly organized nature of the fibers[17] to give the observed (non-amyloid) color in cross-polarized light.

Thus, the standard SAF preparations cannot be considered β-structure-based or amyloid-like. Rather, and consistent with foregoing CD spectroscopy and X-ray fiber-diffraction[16,17] and the FT-IR reported here, they are α-helical as designed. Regarding the morphologically different SAF−MaP mixtures; however, these had some tinctorial properties characteristic of amyloid-like assemblies. Furthermore, longer incubations of these samples with Congo Red resulted in a distinctive pattern in which the fibers showed an intense red color with localized yellow-green areas (Figure 8C). Such areas were evenly

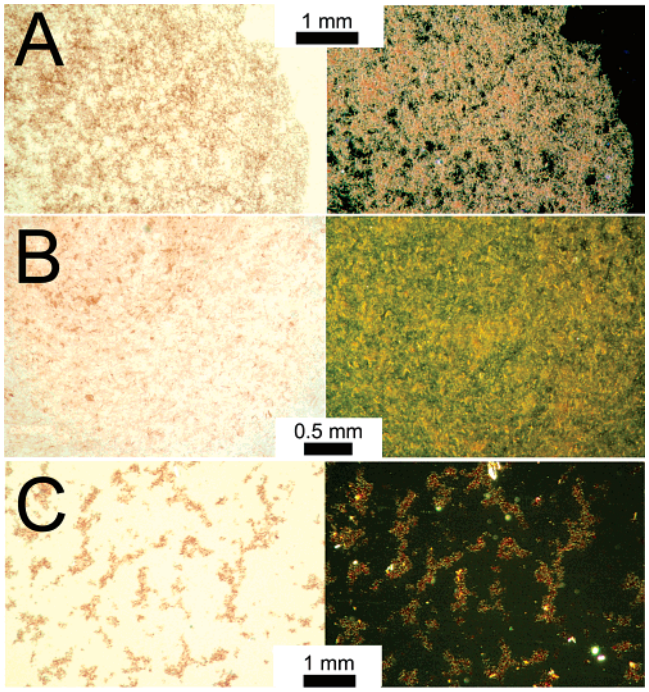

Figure 8. Light (left column) and polarized light (right column) microscopy images of SAF (A) and SAF−A^{N}C^N (B, C) fibers stained with Congo Red. In images A and B, fibers were formed at standard conditions and stained for 24 h. In image C, the staining of SAF−A^{N}C^N fibers was prolonged to 36 h.

distributed across the fibers with negligible background contamination. This suggests that the yellow-green inclusions correspond to the sites of at least partly β-structured peptides.[21] Our supposition is that MaP peptides are incorporated at these points and that these peptides either bind Congo Red in a similar way to amyloid or that they introduce amyloid-like structures locally.

Thus, both α-helical and β-sheet conformations may coexist in SAF−MaP mixtures. In some other fibrillar systems conformational switches have been observed at elevated temperatures.[23] To probe this possibility, we followed the thermal denaturation of SAFs and SAF−MaP mixtures by CD spec-

(20) (a) Surewicz, W. K.; Mantsch, H. H.; Chapman, D. *Biochemistry* **1993**, *32*, 389−394. (b) Heimburg, T.; Schuenemann, J.; Weber, K.; Geisler, N. *Biochemistry* **1996**, *35*, 1375−1382.
(21) (a) Glover, J. R.; Kowal, A. S.; Schirmer, E. C.; Patino, M. M.; Liu, J. J.; Lindquist, S. *Cell* **1997**, *89*, 811−819. (b) Horwich, A. L.; Weissman, J. S. *Cell* **1997**, *89*, 499−510.
(22) (a) Inouye, H.; Nguyen, J. T.; Fraser, P. E.; Shinchuk, L. M.; Packard, A. B.; Kirschner, D. A. *Amyloid* **2000**, *7*, 179−188. (b) Khurana, R.; Uversky, V. N.; Nielsen, L.; Fink, A. L. *J Biol. Chem.* **2001**, *276*, 22715−22721.
(23) (a) Zhang, S.; Rich, A. *Proc. Natl. Acad. Sci. U.S.A.* **1997**, *94*, 23−28. (b) Ciani, B.; Hutchinson, E. G.; Sessions, R. B.; Woolfson, D. N. *J. Biol. Chem.* **2002**, *277*, 10150−10155.

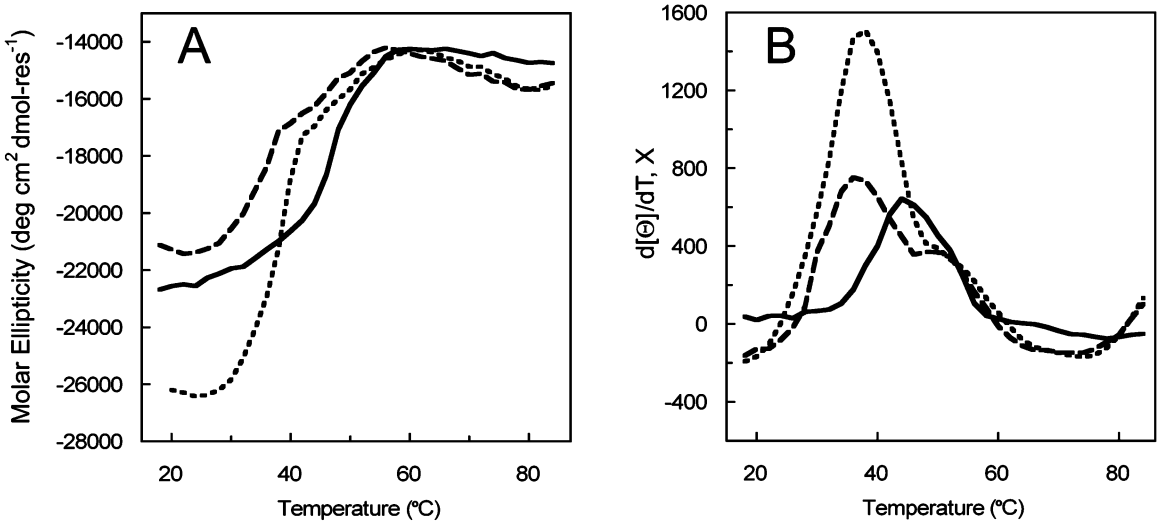

Figure 9. Thermal unfolding curves (A) and their first derivatives (B) of SAF-only (solid line) and A^NC^N-containing (dashed and dotted lines) fibers. The curves were recorded at 222 nm (solid and dashed lines) and at 225 nm (dotted lines).

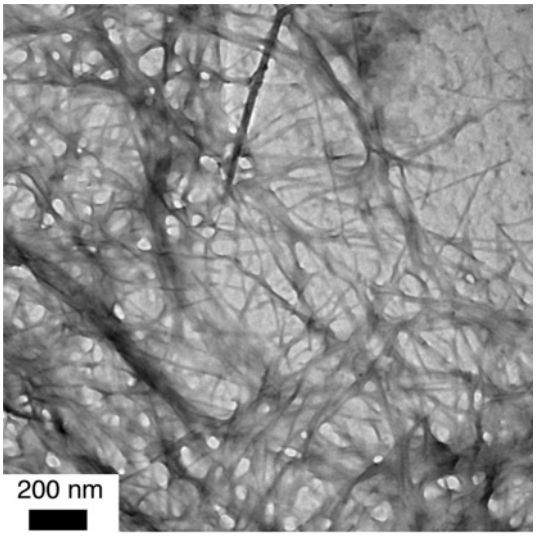

Figure 10. Electron micrographs of the thermally denatured SAF−A^NC^N matrix.

troscopy. The denaturation of standard SAFs gave sigmoidal unfolding curves with transition midpoints (T_M) of 44 ± 2 °C (Figure 9). This suggests cooperative folding by a single or small number of closely related fiber types. To test how the incorporation of MaP peptides affected thermal unfolding, we performed similar experiments on A^NC^N-containing fibers. These unfolded with partly sigmoidal transitions and sharp kinks just below 40 °C (Figure 9A). This implies either some refolding analogous to that observed in other systems[23] or that two or more thermodynamically distinct types of fibers are present. Indeed, the first derivatives of the SAF−A^NC^N denaturation curves suggested two stability populations in the assembly (Figure 9B). After cooling, the CD and FT-IR spectra revealed irreversible denaturation of the α-helical structure and refolding to the β-structure (Figure 7). Therefore, the thermally denaturated fibers had undergone conformational reorganization. This is supported by TEM of the melted and cooled samples, which showed matrices of very tightly connected or fused fibers (Figure 10). Subsequent melting experiments of these samples failed to give sigmoidal transitions or clear transition midpoints (results not shown).

In conclusion to this section, freshly assembled SAF fibers contain predominantly α-helical secondary structure. The addition of MaP peptides compromises this slightly and introduces regions of β-structure, which is possibly amyloid-like. Heating the standard SAFs and MaP-containing SAF preparations results in irreversible denaturation and the formation of very different fiber morphologies consistent with entangled amyloid-like structures.

Summary

We have introduced a novel approach to the bottom-up assembly of nanometer-to-micron scale fibrous matrices. This work builds on our earlier studies in which two complementary peptides, SAF-p1 and SAF-p2a, co-assemble to form linear, nonbranched protofibrils. In turn, these mature and thicken to fibers tens of nanometers thick and tens of microns long, which we call SAFs.[16] The new work adds the MaP (Matrix-Programming) peptides to the SAF system. MaP peptides are essentially half-sized fragments of SAF peptides conjugated together to form two- or three-limbed constructs. Thus, MaP peptides have elements that are complementary to the original SAF peptides for incorporation into the growing SAFs, plus elements to spawn branches and interprotofibril links, which result in connections between the matured fibers; in other words, MaP peptides are hubs for altering fiber morphology at a supramolecular level. A number of MaP peptides have been engineered, and in combination with the original SAF peptides, they form hyperbranched networks, polygonal matrices, and regularly segmented fibers.

In more detail, the original SAF peptides each have two distinct halves: SAF-p1 comprises A^N and B^C and SAF-p2a comprises C^N and D^C, where A^N complements D^C and B^C complements C^N. These half-peptide units are the building blocks for the MaP peptides. Different combinations of these building blocks render different MaP peptides. Interestingly, the different MaP peptides produce different fiber morphologies when added to mixtures of the standard SAF peptides. For example, the $A_2{}^NB^C$ combination produces hyperbranched fibers (Figure 2D); A^NC^N produces interconnected networks (Figure 5); and $B_2{}^C$ produces segmented fibers (Figure 3B and C). Themes emerge from our observations that link the chemistry

of the MaP peptides to the morphological feature(s) that they produce. For instance, MaP peptides containing the C^N block tend to form kinked structures, and those with the B^C block tend to form segmented or intermitted fibers and fiber networks (Figure 3). It is more difficult to assign precise roles for A^N and D^C blocks: they appear to be more promiscuous in their interactions and with the effects; for example, fiber kinking, splitting and/or branching are all seen concomitantly with MaP peptides containing these blocks. These themes can be understood in terms of the following relatively straightforward model: the B^C and C^N blocks were designed to form weak but highly specific coiled-coil interactions. This is because each has an interfacial asparagine residue, which must be complemented by another such residue in any peptide−peptide interaction. Essentially, this makes the B^C:C^N interaction the obligate pairing for these two blocks, which restricts the type of morphological feature produced. On the other hand, the A^N and D^C blocks do not have such asparagine inclusions and, as a result, make potentially stronger but more promiscuous peptide−peptide interactions. This is a kinetic argument: A^N and D^C have the strongest potential pairwise interaction and probably get sequestered within the heterodimer interfaces and buried within protofibils faster than B^C and C^N; this would leave the ends of the growing protofibrils and fibers with predominantly B^C and C^N overhangs, which would have a preference for incoming heterodimers also cemented by A^N:D^C interactions and with B^C and C^N overhangs. However, because of their opposite charges, the A^N and D^C blocks of free peptides may also interact to some extent with the overhanging B^C and C^N blocks, respectively, of the growing fibers. This leads to A^N- and D^C-containing FiSh and MaP peptides' potential for being promiscuous and forming more than one morphological feature.

Extending this argument, a final part of our developing model for SAF fibrillogenesis is that the protofibrils extend more productively from one end than the other. Again, because the A^N:D^C interaction is stronger than B^C:C^N, the majority of nucleating SAF-p1:SAF-p2a heterodimers will leave B^C and C^N overhangs, Figures 1 and 4. On the basis of our experience with the SAFs, we propose that C^N overhangs propagate fibrillogenesis better than B^C ends. Therefore, C^N-containing MaP peptides, such as $C_2{}^N$, can add to fibers and continue assembly uninterrupted; in contrast, those based on B^C, like $B_2{}^C$, add to the C^N growing ends and may stall or even block fibrillogenesis causing intermissions in the matured structures. This would explain several of our findings, including the observation of segmented fibers formed with $A^NB_2{}^C$ and $B_2{}^C$; whereas $C_2{}^N$ simply kinks otherwise normal full-length fibers.

Thus, by making appropriate combinations of half-peptide building blocks in the SAF system, fiber morphology can be tailored to a considerable extent; that is, peptide self-assembly and fibrillogenesis can be programmed from the bottom up to generate novel systems of increased complexity. In our view, this represents an advance in controlling peptide-based self-assembly and potentially a powerful route to novel designs for peptide-based materials.

Experimental Section

Peptide Synthesis and Mass Spectrometry. All peptide synthesis reagents and resins were purchased from Applied Biosystems (Warrington, UK) or CN Biosciences (Nottingham, UK). Peptides were assembled on a Pioneer Peptide Synthesis System (PE Applied Biosystems, CA) using standard Fmoc/*t*Bu solid phase protocols on PEG-PS-resin with TBTU/DIPEA as coupling reagents. Orthogonally conjoined constructs were made through lysine or glutamate residues on resin and/or manually using combinations of Fmoc/*t*Bu/Mtt or Fmoc/*t*Bu/Aloc protection schemes. For some peptide blocks a glutamine residue was replaced by tyrosine to allow accurate concentration determination by UV spectroscopy. Dendritic spacers were used as hubs for all the constructs as follows: $(\beta Ala)_3$-Lys$(\beta Ala)_3$-NH_2 for $A_2{}^N$ and $C_2{}^N$; Glu$(\beta Ala)_3$-$(\beta Ala)_3$ for $B_2{}^C$ and $D_2{}^C$; $(\beta Ala)_3$-Lys$(\beta Ala)_3$-$(\beta Ala)_3$ for $A_2{}^NB^C$, $C_2{}^ND^C$, $C_2{}^NC^C$, and $C^NC^CD^N$; $(\beta Ala)_3$-Glu$(\beta Ala)_3$-$(\beta Ala)_3$ for $A^NB_2{}^C$; $(\beta Ala)_4$-Lys$(\beta Ala)_3$-Lys$(\beta Ala)_3$-NH_2 for $A_3{}^N$ and $C_3{}^N$. Peptides were purified by semipreparative RP-HPLC on a JASCO HPLC system (model PU-980, Tokyo, Japan) using Vydac C_8 semipreparative (5 μM, 10 mm i.d. × 250 mm) columns and confirmed by MALDI-Tof mass spectrometry (Micromass Ltd, Manchester, UK) with α-cyano-4-hydroxycinnamic acid as the matrix.

MS $[M+H]^+$: SAF-p1 - *m*/*z* 3174 (calc), 3175 (found); SAF-p2a - *m*/*z* 3325 (calc), 3326 (found); $A_2{}^N$ - *m*/*z* 3686 (calc), 3687 (found); $B_2{}^C$ - *m*/*z* 3841 (calc), 3842 (found); $C_2{}^N$ - *m*/*z* 4166 (calc), 4167 (found); $D_2{}^C$ - *m*/*z* 3663 (calc), 3663 (found); $A_2{}^NB^C$ - *m*/*z* 5463 (calc), 5465 (found); $A^NB_2{}^C$ - *m*/*z* 5541 (calc), 5543 (found); $C_2{}^ND^C$ - *m*/*z* 5855 (calc), 5857 (found); $C_2{}^NC^C$ - *m*/*z* 6108 (calc), 6110 (found); $A_3{}^N$ - *m*/*z* 5784 (calc), 5787 (found); $C^NC^CD^N$ - *m*/*z* 5855 (calc), 5856 (found); $A_3{}^N$ - *m*/*z* 5784 (calc), 5787 (found); $C_3{}^N$ - *m*/*z* 6505 (calc), 6507 (found). The doubly $[M + 2H]^{2+}$ and triply $[M + 3H]^{3+}$ charged ions along with Na^+ and K^+ salt species were also presented.

Fiber Assembly. Fiber samples (200 μL) were prepared by mixing aqueous solutions of SAF peptides (to a final concentration of 100 μM in each peptide), with MaP peptides added in the ratios given in the text. The solutions obtained were incubated overnight at 20 °C in filtered (0.22 μM) 10 mM MOPS, pH 7−7.4. SAF-only fibers were used as controls.

Transmission Electron Microscopy. After incubation, 8 μL drops of peptide solutions were applied to a carbon-coated copper specimen grids (Agar Scientific Ltd, Stansted, UK) and dried with filter paper. The grids were stained with filtered (0.22 μM) 0.5% aqueous uranyl acetate for electron microscopy as described elsewhere[15] at 20 °C and were examined in a Hitachi-7100 TEM at the accelerating voltage of 100 kV. Exposure times were predominantly within 3 min, but could safely be varied up to 20 min, with beam spot sizes being 4 and 6 (0.3−8 μm in eight steps). Images were digitally acquired with an axially mounted (2K × 2K pixel) Gatan Ultrascan 1000 CCD camera (Gatan UK, Oxford, UK) and analyzed with the proprietary software.

Congo Red Staining. Assembled SAF and SAF-MaP preparations (50 μL) were incubated with Congo Red (2.5 μM)[23] at 20 °C over 24 h (unless stated otherwise). The stained preparations were then visualized by light microscopy using both plain and polarized light.

Circular Dichroism Spectroscopy was performed on a JASCO J-715 spectropolarimeter fitted with a Peltier temperature controller as published elsewhere[15b] using 100 μM peptide solutions at pH 7−7.4, and at 20 °C, unless stated otherwise. The concentration of peptide bonds was taken as 54 μM ((2 · (28−1)) · 100 μM) for all spectra and neglected any contribution to CD from the specialist (MaP/FiSh) peptides. The thermal denaturation curves were recorded at 1 °C intervals using a 1-nm bandwidth, averaging the signal for 16 s and with at 1 °C/min ramp rate.

Fourier Infrared Spectroscopy was carried out on a thermostated Bruker Tensor 27 (BioATR) spectrometer using a ZnSe ATR crystal with a Teflon coat. The spectra (200 interferograms) were recorded in the range 400−4000 cm^{-1} with a spectral resolution of 2 cm^{-1}. All spectra were recorded at 20 °C. Acquired data were processed using proprietary software (OPUS) according to the manufacture protocols.

Acknowledgment. We thank the BBSRC of the UK for financial support (E13753 and BBS/B/04676) and members of the D.N.W. group for helpful discussions.

JA052972I